Simulation of Green Water Loading Using the Navier-Stokes Equations

Fekken, G.; Veldman, A.E.P.; Buchner, B.

SIMULATION OF GREEN WATER LOADING USING THE NAVIER-STOKES EQUATIONS

G. Fekken[1], A.E.P. Veldman[1]
B. Buchner[2]
[1]University of Groningen, Department of Mathematics,
P.O. Box 800, 9700 AV Groningen, The Netherlands
E-Mail: G.Fekken@math.rug.nl
[2]Maritime Research Institute Netherlands (MARIN)
P.O. Box 28, 6700 AA Wageningen, The Netherlands
E-mail: B.Buchner@marin.nl

ABSTRACT

Simulating viscous flows with a free surface causes special difficulties, since its position will change continuously. Therefore, besides solving the Navier-Stokes equations, the position of the free surface must be determined every time step. In the present method, the Navier-Stokes equations are solved on a three-dimensional Cartesian grid. A Volume-of-Fluid function is used for the position of the fluid. Since the method is able to handle arbitrary forms of the geometry, many types of industrial flow problems can be simulated. In this paper the problem of green water loading on the foredeck of a ship is discussed and a comparison is made with experimental results. Waterheights, pressures and water contours are produced and compared with model tests. Also forces on different structures placed on the deck are compared and analyzed.

INTRODUCTION

When a ship at sea is sailing or moving in the waves, it may get water on the foredeck. This water, which flows on the deck in high waves when the relative wave motion around the bow is exceeding the deck level, is called *green water*. As a result of this green water loading, damage to superstructures on the deck is still a common occurrence. The Maritime Research Institute Netherlands (MARIN) has done extensive model test research to this phenomenon during the last few years [1], [2]. In the paper a simulation method will be described with which this phenomenon can be investigated numerically.

The simulation of green water flow on the foredeck of a ship is a complex problem, since the water will behave wildly when it flows on the deck, causing effects like air bubble entrapment. The tests also show complex high velocity flow patterns on the deck. Besides the model test research MARIN has done, it also investigated the non linear relative wave motions around the bow with a boundary integral method, modeling the flow with a potential function [3]. However, fluid flow is best described by the complete Navier-Stokes equations. In 1995, at the University of Groningen (R*u*G), the development of a computer program called ComFlo has been started which can solve fluid flow with free surfaces in 3D-complex geometries. Here the Navier-Stokes equations are solved on a Cartesian grid. No motion of the geometry has been implemented yet, so this will cause some differences between the tests and the simulation. The inflow conditions at the boundaries of the domain will be determined by the data of the model tests instead of simulating an incoming wave.

MATHEMATICAL MODEL

The motion of water, and in general the motion of a viscous, incompressible fluid can be described by the incompressible Navier-Stokes equations, consisting of conservation of mass and conservation of momentum:

$$\nabla \cdot \boldsymbol{u} = 0 \qquad (1)$$

$$\frac{\partial \boldsymbol{u}}{\partial t} + (\boldsymbol{u} \cdot \nabla)\boldsymbol{u} = -\frac{\nabla p}{\rho} + \nu \Delta \boldsymbol{u} + \boldsymbol{F} \quad (2)$$

where $\boldsymbol{u} = (u, v, w)$ is the velocity, ρ is the density, p is the pressure, ∇ is the gradient operator, $\nabla \cdot$ is the divergence operator, and Δ is the Laplace operator. Further ν is the kinematic viscosity and $\boldsymbol{F} = (F_x, F_y, F_z)$ is an external body force, e.g. gravity.

Further, boundary conditions are required for the solid boundary, the free surface and eventually in- and outflow boundaries. At the solid boundary a no-slip condition is used: $\boldsymbol{u} = 0$.

Free-slip walls are also possible, resulting in the conditions $u_n = 0$ and $\tau = 0$. Here $u_n = \boldsymbol{u} \cdot \boldsymbol{n}$ is the component of the velocity perpendicular to the wall, $\tau = \frac{\partial u_t}{\partial n}$ is the tangential stress, where u_t is the velocity component in the tangential direction.

At the free surface the boundary conditions consist of two components:

$$-p + 2\mu \frac{\partial u_n}{\partial n} = -p_0 + 2\gamma H \qquad (3)$$

$$\mu \left(\frac{\partial u_n}{\partial t} + \frac{\partial u_t}{\partial n} \right) = 0 \qquad (4)$$

where μ is the dynamic viscosity, p_0 is the atmospheric pressure, γ is the surface tension and $2H$ is the total curvature of the surface. These boundary conditions describe the continuity of normal and tangential stresses at the free-surface. Further, for the free surface displacement an equation is required: Suppose the position of the free surface is described by $s(x, t) = 0$, then the movement of the free surface becomes

$$\frac{Ds}{Dt} = \frac{\partial s}{\partial t} + \boldsymbol{u} \cdot \nabla s = 0. \qquad (5)$$

At inflow boundaries the velocity $\boldsymbol{u}$ is prescribed, and at outflow boundaries the homogeneous Neumann condition $\frac{\partial \boldsymbol{u}}{\partial n}$ is used. This is better than prescribing the normal component of the velocity, since then a boundary layer could easily be created. Further, at outflow boundaries the pressure p is set equal to the atmospheric value p_0.

NUMERICAL MODEL

In this section the mathematical model will be discretized to obtain a numerical model.

Description of geometry and free surface

First a Cartesian grid is laid over the three dimensional domain. The discretization is done on a totally staggered grid, which means that the pressure will be set in the cell centers and the velocity components in the middle of the cell faces between two cells (figure 1). Like all figures of the discretization of geometries in this paper, this is a 2-dimensional example. Extension to 3D is straightforward.

Since complex geometries are used, the grid cells will run through the boundaries in several ways. This is also the case for the free surface, with an extra complexity since the free surface is time-dependent. Also the main reasons why Cartesian grids are used, can be inferred from this. In the first place each cell has the same orientation which is an advantage with respect
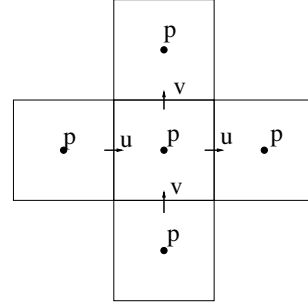

Figure 1: Location of the pressure and velocity components

to the transportation of the free surface. In the second place when the geometries become more complex, the creation of boundary-fitted grids will become very complex and time consuming. A disadvantage of the Cartesian approach is the discretization of the boundary conditions, since in general the grid will not be fitted in the boundary. Now the method which takes care of the complex shape of the geometry and the free surface is discussed.

Apertures

An indicator function is used in the form of so-called *apertures*, which are divided into two classes:

1. volume apertures

   In every cell, the geometry aperture F_b defines the fraction of the cell where fluid is able to flow. The (time-dependent) fluid aperture F_s defines the fraction of the cell which is occupied by fluid. Of course $0 \leq F_s \leq F_b \leq 1$.

2. edge apertures

   The edge apertures A_x, A_y, A_z define the fraction of a cell surface which is contained in the flow domain, so A_x indicates the fraction of the cell surface through which fluid is able to flow in x-direction, A_y in y-direction and A_z in z-direction.

Figure 2 shows a 2-dimensional example of a grid cell using apertures. Here $F_b = F_b \setminus F_s + F_s = 0.8$.

Labels

After calculating the apertures, every cell will be given a *cell label*, to make distinction between the boundary, the fluid and the air, and because the pressure is treated differently near the wall and near the free surface. Since the free surface is time-dependent, two classes of labeling are introduced,:
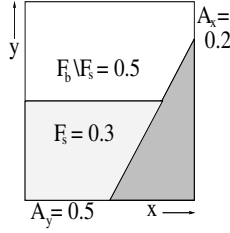
Figure 2: Example of a grid cell with geometry and fluid apertures

1. geometry cell labels

   This labeling class is time-independent, consisting of three different labels:
   - **F**-cells: All cells with $F_b \geq \frac{1}{2}$
   - **B**-cells: All cells adjacent to an **F**-cell
   - **X**-cells: All remaining cells

2. free-surface cell labels

   Free-surface labels are time-dependent and they are a subdivision of the **F**-cells:
   - *E*-cells: All cells with $F_s = 0$
   - *S*-cells: All cells adjacent to an *E*-cell
   - *F*-cells: All remaining **F**-cells

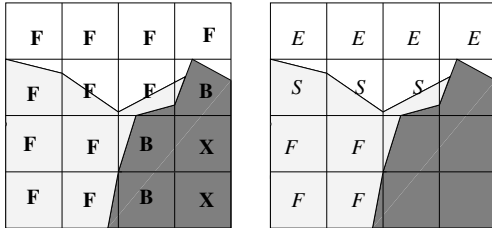Figure 3 shows an example of this labeling.

Figure 3: Example of geometry cell labeling (left) and free-surface cell labeling (right)

For the treatment of the velocity, the velocities between cells have to be labeled, too. So we introduce *velocity labels*, which, like the cell labels, have to be subdivided in a time-dependent and a time-independent class:

1. geometry velocity labels

   These (time-independent) labels are a combination of the labels of the geometry where the velocities lie in between. Five combinations are possible: **FF, FB, BB, BX** and **XX.**

2. free-surface velocity labels

   These labels are time-dependent and they are a combination of the labels of the free surface. The following combinations are possible: *FF, FS, SS, SE, EE, FB, SB* and *EB*.

Further, there is one more class of labeling, namely inflow and outflow labels, resp. **I**- and **O**-cells. They are just a specific subset of the **B**-cells.

Discretization of the Navier-Stokes equations

When all cells and velocities are labeled, the Navier-Stokes equations can be discretized in time and in space. First the Navier-Stokes equations are written more simplified as:

$$\nabla \cdot \boldsymbol{u} = 0 \qquad (6)$$
$$\frac{\partial \boldsymbol{u}}{\partial t} + \nabla p = \boldsymbol{R} \qquad (7)$$

Here $\frac{p}{\rho}$ is replaced by p (ρ is normalized to 1) and $R = \nu \Delta \boldsymbol{u} - (\boldsymbol{u} \cdot \nabla)\boldsymbol{u} + \boldsymbol{F}$, containing all convective, diffusive and body forces.

Discretization in time

The explicit first order Forward Euler method is used:

$$\nabla \cdot \boldsymbol{u}^{n+1} = 0 \qquad (8)$$
$$\frac{\boldsymbol{u}^{n+1} - \boldsymbol{u}^n}{\delta t} + \nabla p^{n+1} = \boldsymbol{R}^n \qquad (9)$$

Here $n + 1$ and n denote the new and old time level respectively, and δt is the time step. Equation (8) and the pressure in (9) are treated on the new time level, to make sure the new $\boldsymbol{u}$ is divergence free.

Discretization in space

The spatial discretization can be explained using the scheme in figure 4.
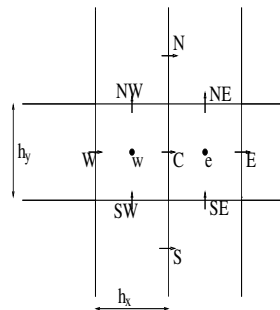

Figure 4: Discretization scheme

Equation (8) is applied in the centers of the cells and a central discretization is used. In the cell with center w the discretized equation becomes:

$$\frac{u_C^{n+1} - u_W^{n+1}}{h_x} + \frac{v_{NW}^{n+1} - v_{SW}^{n+1}}{h_y} = 0 \qquad (10)$$

The momentum equation (9) is applied in the centers of the cell faces, for instance the discretization in point C becomes:

$$\frac{u_C^{n+1} - u_C^n}{\delta t} + \frac{p_e^{n+1} - p_w^{n+1}}{h_x} = R_C^n. \qquad (11)$$

The diffusive terms in R_C^n are discretized centrally, and for the convective terms upwind or central discretization is possible. For wildly moving fluids mostly an upwind discretization is used, since central discretization may cause stability problems (see [4] section 2.4).

Discretization near the free surface

Near the free surface besides F-cells, S-cells and E-cells appear. In E-cells the pressure is set to the atmospheric value p_0. In S-cells the pressure is determined by linear interpolation between the pressure in F-cells and the free surface. The pressure p_F in F-cells is obtained from the pressure Poisson equation which is handled in the next section. The pressure at the free surface p_f is obtained from equation (3), where the term $2\mu \frac{\partial u_n}{\partial n}$ is neglected because μ is small in relation to the other terms. So $p_f = p_0 - 2\gamma H$. The pressure p_S now becomes

$$p_S = \eta p_f + (1 - \eta) p_F. \qquad (12)$$
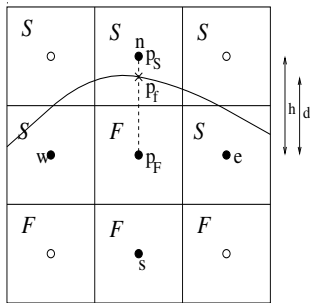
Here $\eta = \frac{h}{d}$ (figure 5).

Figure 5: Pressure interpolation in S-cells

For the velocities in equation (4) there are a number of possibilities. The velocities *FF, FS* and *SS* are obtained solving the momentum equations. But when discretizing derivatives *SE-* and *EE-* velocities are needed. *SE*-velocities are computed by demanding mass conservation in the corresponding S-cell. This velocity can then be computed from the five other (not unknown) velocities appearing in the equation for mass conservation. However, it is possible that two or more of these velocities are *SE*, in which case other decisions have to be made, e.g. setting derivatives like $\frac{\partial u}{\partial x}$ to zero. *EE*-velocities not surrounded by at least one *SS*-velocity are set to zero. Other *EE*-velocities are computed using the discrete simplified version of 3, existing of equations like

$$\frac{\partial u}{\partial z} + \frac{\partial w}{\partial x} = 0 \qquad (13)$$

The determination of these velocities is more extensively treated in [5].

In- and outflow discretization

In- and outflow cells are a specific subset of the **B**-cells.

- Inflow
  The velocity between an **I**-cell and an **F**-cell gets a prescribed value and is labeled as **FI**.

- Outflow
  In an **O**-cell two velocities have to be labeled: **FO** and **OX**. The **FO**-velocity is computed from the momentum equations and then the **OX**-velocity is set equal to the **FO**-velocity, to satisfy the condition $\frac{\partial \boldsymbol{u}}{\partial n} = 0$.

Figure 6: In- and outflow cells

The pressure Poisson equation

The pressure p^{n+1} in (9) has to be determined in such a way that equation (8) holds. This can be attained by substituting (9) into (8), resulting in the following equation:

$$\Delta p^{n+1} = \nabla \cdot \left(\frac{\boldsymbol{u}^n}{\delta t} + \boldsymbol{R}^n \right) \qquad (14)$$

This equation is known as the Poisson equation for the pressure. No boundary conditions for the pressure are available for this equation, since they only involve the velocity $\boldsymbol{u}$. Therefore we first discretize equations 8 and 9, and then substitute the boundary conditions

for u, and after that we substitute these discretized equations to create the discretized Poisson equation. It will follow that no more boundary conditions for the pressure are required now (see [4] section 4.4).

After discretization it follows that the discrete analogon for the Laplace operator (Δ) consists of a central coefficient C_p and six coefficients C_n, C_s, C_w, C_e, C_u and C_d, related to the six neighbouring cells. When we denote the right hand side of (14) by f_p, the Poisson equation can be written as:

$$C_p p_p + C_n p_n + C_s p_s + C_e p_e + C_w p_w + \\ C_u p_u + C_d p_d = f_p \quad (15)$$

The Poisson equation is solved by SOR-iteration (Successive Over Relaxation), which has some advantages:

- simple implementation, immediately using every new value.
- easy vectorization and parallelization, using a Red-Black ordening of the cells.
- rapid convergence, using an automatically adjusted relaxation parameter ω [6].

When the SOR-iteration has finished the pressure in every cell is known at the new time step, and the new velocities can now be computed.

Free surface displacement

When the velocities at the new time step are known, the free surface can be displaced. The sequence of actions that have to be done to achieve this are:

1. *compute fluxes between cells*
   The fluxes between cells are computed by velocity times the area of the cell, taking into account the edge apertures.

2. *compute new fluid apertures F_s*
   Using the fluxes between the cells, the new F_s can be computed.

3. *adjust free-surface labeling*
   When the new fluid apertures are known the free-surface labeling can be adjusted.

This algorithm is called the Donor-Acceptor algorithm, which means that fluid is transported from a donor cell to an acceptor cell. A few things have to be taken into account: A donor cell cannot loose more fluid than it contains and an acceptor cell cannot receive more fluid than the amount of flow space that is available in the cell. Further, in S-cells the fluid has to stay coherent, which is accomplished by making use of a local height function (see [7]).

The CFL-number

One can imagine that when the fluid is moving very wildly, the time step has to be smaller than when the fluid is moving very calm. It would be useful to adjust the time step to these changes, to achieve an improvement in the computation time. Therefore the Courant-Friedrichs-Levy number (CFL-number) is introduced:

$$CFL = \frac{|u|\delta t}{h_x} + \frac{|v|\delta t}{h_y} + \frac{|w|\delta t}{h_z} \quad (16)$$

Here h_x, h_y and h_z denote the distances between the cell centers in x-, y- and z-direction. The condition to keep the computation stable, which can be proved by Fourier analysis (see [4]), turns out to be $CFL \leq 1$. This means that the fluid is transported over no more than one cell in one time step, which corresponds with our intuitive approach of stability. In ComFlo the maximum of the CFL-number over all cells is determined, and with respect to this number the time step is adjusted: The time step is immediately halved when the CFL-number becomes larger than a certain constant $C_1 < 1$, and the time step is doubled when the CFL-number is smaller than another constant C_2 which is small enough to be sure the time step can be doubled; typically $C_1 = 0.5$ and $C_2 = 0.1$.

RESULTS

Now the results of the green water simulations, computed by ComFlo will be presented and compared with experimental results. First the initial conditions used in the simulation will be explained. Then the results of the simulation of green water loading, consisting of water heights on the deck, the pressure at one place on the deck and contours of the waterfront will be discussed. Finally, the results of pressures and forces on different structures placed on the deck will be compared with experiments and analyzed. A detailed description of the physical behaviour of green water can be found in [1], [2].

Initial conditions

It will be clear that the simulation of a moving bow in large waves is a complex problem. Since the first goal was to investigate the possibilities to predict the behaviour of the green water on the deck using a numerical simulation program, simpler boundary conditions have been used for a first start.
Examining the situation of green water flow on the deck, a good resemblance for this appeared to be the theoretical dambreak problem (see [1]): A wall of water is placed around the bow and at time zero the water starts to flow onto the deck. Therefore this

dambreak problem was used as an initial condition for the green water problem on the deck. To compare the results of simulations and model tests carried out by MARIN [1], the precise configuration of the dambreak problem had to be adjusted to the data of the tests. This means that this configuration had to be tuned, to create more or less the same results with respect to the contour plots of the progressing water-front on the deck and heights at different positions at the deck. In the future the model will be extended with realistic deck(ship) motions and realistic inflow.

One of the model tests was chosen to be approximated, namely the regular wave test with a bow flare angle of 30 degrees, wave amplitude of 8.65 m and wavelength/shiplength = $\frac{\lambda}{l} = 0.75$. The width of the deck was 47 m and it was approximated by a parabola as shown in figure 7. More details on the tests can be found in [1].

A reasonable approximation for the test mentioned before, seemed to be the dambreak problem with a vertical wall of water of 13 m height at the most forward point of the bow, linearly decreasing to 5 m below the deck level 25 m behind this point (see figure 8). In the simulation no bowflare is used. The total flow domain was a box with dimensions $-40m \leq x \leq 15m, -30m \leq y \leq 30m, -6m \leq z \leq 20m$ where $z = 0$ corresponds with the deck level and $y = 0$ is the symmetry axis. A free-slip boundary condition is used at the sides $y = -30m$ and $y = 30m$. Further, to prevent an upward movement of the water at these sides of the domain, an outflow boundary condition is used from -40 m to -12 m (figure 7). Also an outflow boundary condition is used at the aft wall of the fluid domain where the flow is not interesting. At all other walls of the flow domain no-slip boundary conditions were used.

Green water simulation

The simulation used a uniform grid of 66 x 72 x 32 cells in the x-, y- and z-direction respectively. The computation time was about 4 hours for a duration of 10 seconds full scale on a workstation with a specfp95 of 16.3 and 140 Linpack Mflops. At 30 m from the ships fore perpendicular (fpp) in the middle of the deck a flat vertical structure was placed with a height of 20 m and a width of 15 m. The load on this structure was used as a reference for the load on the other structures. First the heights of the water were measured at three different points at the axis of the deck: at $x = 0$, $x = -10$ and $x = -20$. Further the pressure at the deck was determined at the position $x = -12.5$ (see figure 9).
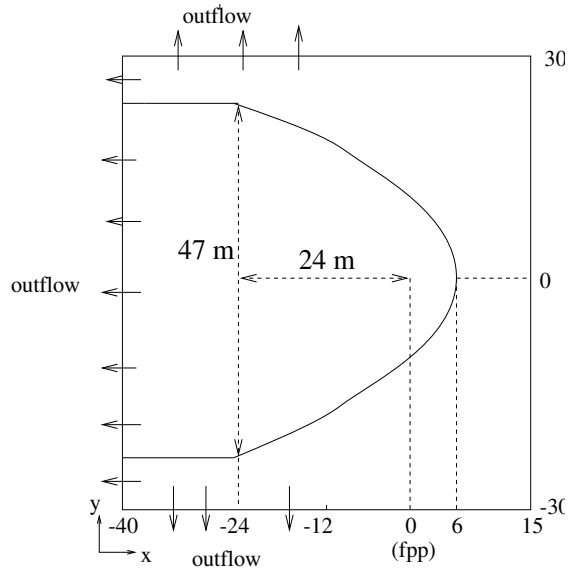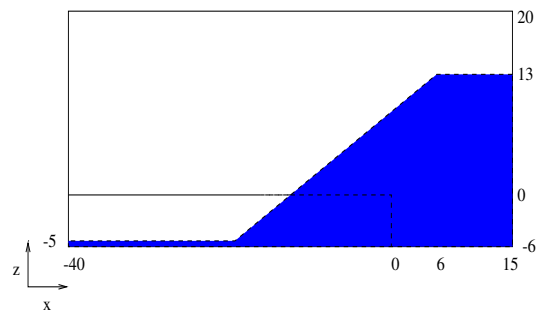

Figure 7: Initial situation in xy-plane
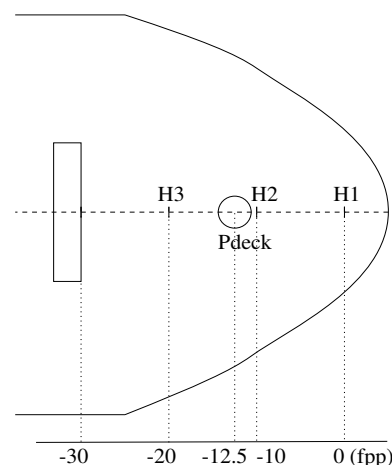

Figure 8: Initial situation in xz-plane

Figure 9: Measure positions for height and pressure

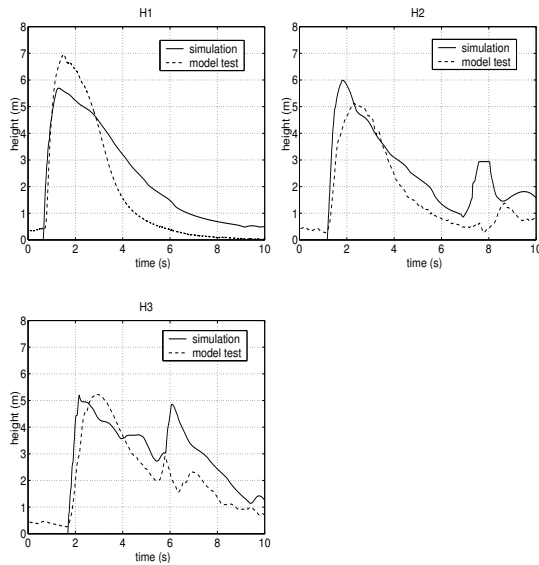The following results are found for the water heights H1 to H3 on the deck:

Figure 10: Results for the heights on the deck

Comparing these results, the resemblance between the model test and the simulation is clear. At H1, H2 and H3 the water rises very quickly and after reaching the maximum height it is slowly going down to a more or less zero value. At H3 a second peak is observed, due to the reflection of the water that was built up in front of the structure. This behaviour is also recognized in the simulation (see snapshot in figure 13 on the next page). A few variations are found in the maximum heights, but the behaviour of the water is quite the same.

To compare both situations also in the transverse direction of the deck, the water contours of the waterfront were plotted in figure 11 (model test) and figure 12 (simulation). The time between the contours is 0.31 seconds.

Having a look at Figures 11 and 12, it is obvious that a high velocity water 'tongue' arises in the middle of the deck both in the simulation and the experiment. However, some differences are observed between the test and the simulation. The waterfront in the simulation seems to be a bit sharper, due to a very shallow part of the front which has no big influence, so this difference looks bigger than it really is. It should also be noted that the contours from the model test are based on visual observation. The contourlines at the sides of the bow are somewhat different too. In the simulation the water almost immediately flows onto the deck around the full bow,
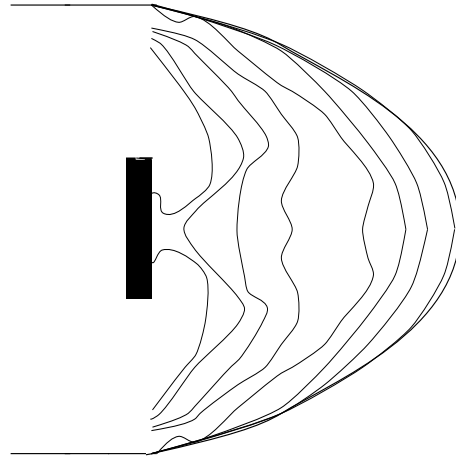
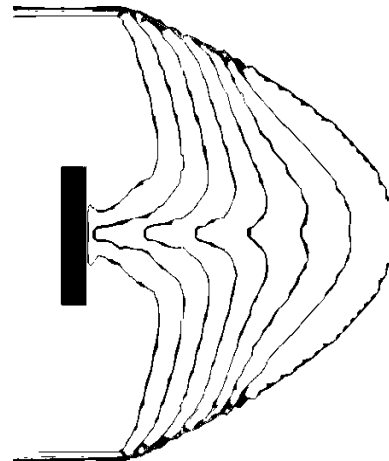Figure 11: Contours of waterfront (model test), time step 0.31 s

Figure 12: Contours of waterfront (simulation), time step 0.31 s

but in the test, likely because of the bowflare that pushes the water away from the bow, the water flows more gradually onto the deck around the bow. Also the vertical and angular motion of the deck can play a role here.

However, the global behaviour is similar, and the heights of the water are comparable, so a further investigation in the behaviour of the green water should be possible with this simulation.

The appearance of the high-velocity water 'tongue' is very well visible in a movie of this simulation, which is shown below, created by the visualization system AVS. Also the impact on the structure and the returning of the water which causes the second

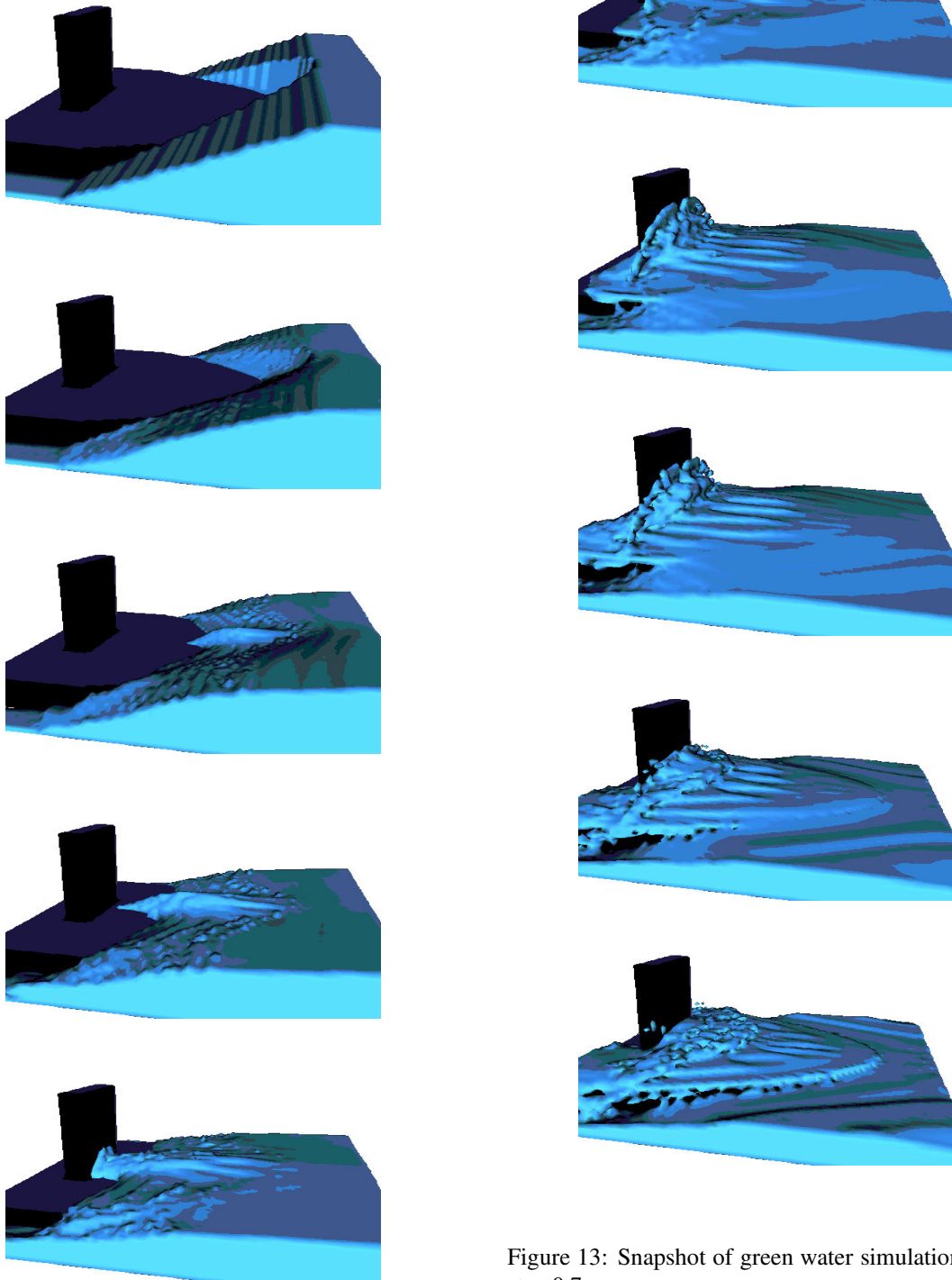maximum in the heights and pressure are clearly visible.

Figure 13: Snapshot of green water simulation, time step 0.7 s

The photos on the next page give an impression of the model test and how the water behaves on the deck in comparison with the simulation. Also the high velocity water 'tongue' is again clearly visible.
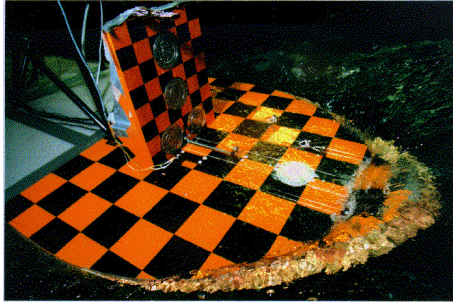
Figure 14: Photos of a model test, time step 0.31 s

Now a comparison between the model test and the simulation is made for the pressure at the deck (figure 15).
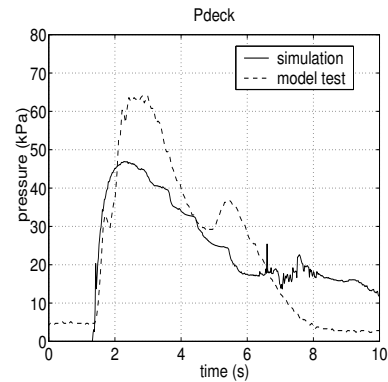

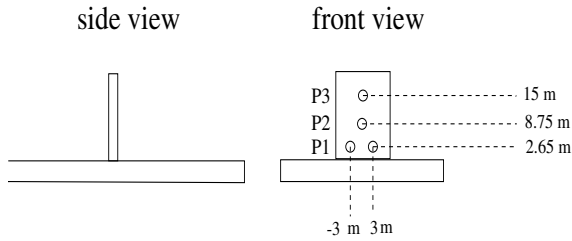Figure 15: Pressures for simulation and experiment

Like the heights, the pressure increases very fast and then, after the maximum pressure is reached, slowly decreases. Since the vertical velocity and acceleration of the deck is not simulated, the pressure for the simulation only exists of a hydrostatic component : $p = \rho g h$. This is the reason why the pressures in the tests are higher than in the simulation. A complete expression for the pressure on the deck, including the effects of the vertical velocity and acceleration can be found in [1]. This pressure will be found when the vertical motion of the deck is included in the method.

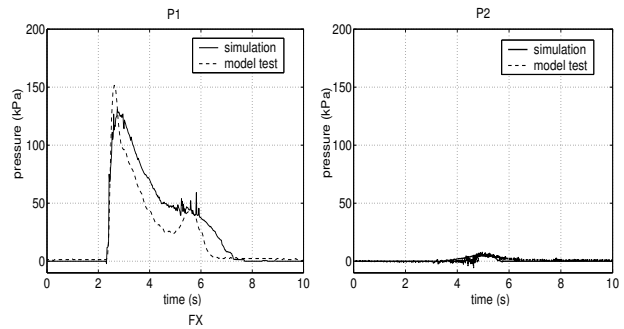**Pressures and forces on different structures**

To determine the effect of different structural shapes on green water loading, MARIN has carried out some model tests with a number of different structures placed on the deck. The following structures were used in the tests (positions are with respect to deck level and the ships centerline):
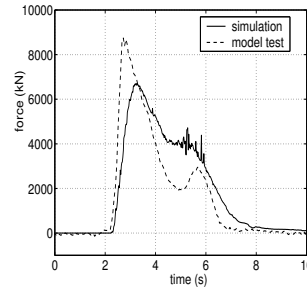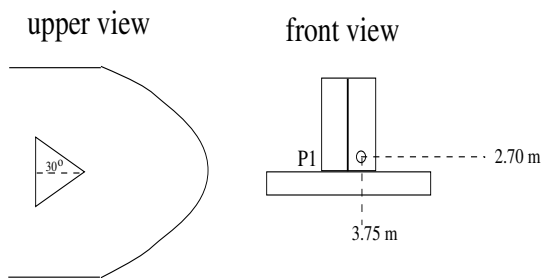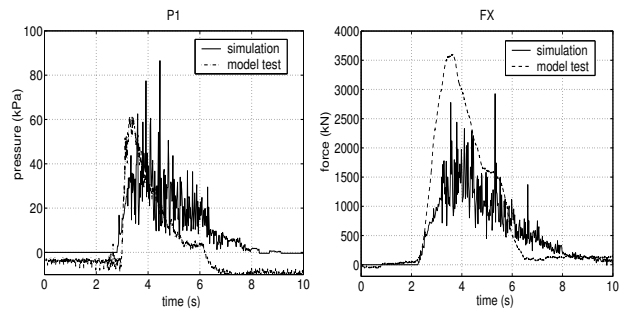
Structure 1: Squared structure

side view   front view

P3 ⊖---------------- 15 m
P2 ⊖---------------- 8.75 m
P1 ⊙ ⊖------------- 2.65 m

-3 m 3 m

Structure 2: Triangular 30 degrees

upper view   front view

30°

P1 ⊖ --------- 2.70 m

3.75 m

Structure 3: Cylindrical front

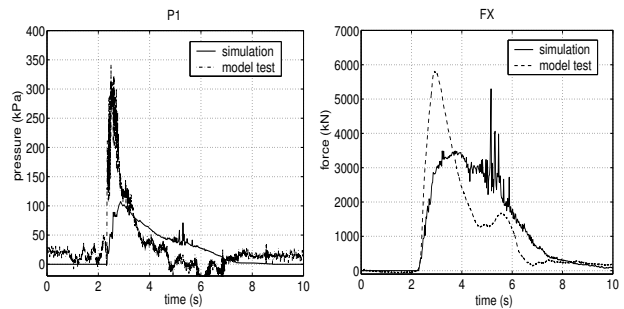upper view   front view

P1 ⊖ ---------- 2.80 m

0 m

Figure 16: Different structures used in the tests

All structures are placed with their front at 30 m from the fore perpendicular, their height is 20 m and their width is 15 m. Pressures are measured at the pressure panel positions which are drawn in the figures (front view), the area of the circular pressure panels (2.7 m diameter) is 5.7255 m^2. Further, the total force in x-direction F_x is measured on every structure.

Below a comparison is made between the pressures and total loads on the different structures.

Structure 1 (squared)

Structure 2 (triangular 30 degrees)
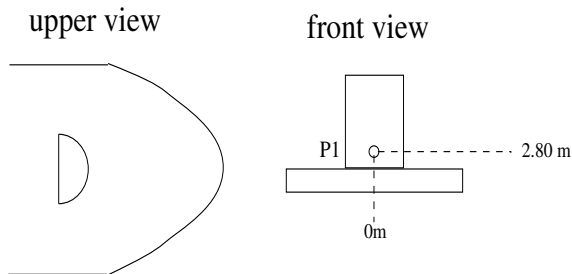
Structure 3 (cylindrical front)

Figure 17: Comparison of measured and calculated pressures and total loads on the different structures

Recapitulating the results of the different structures, it can be concluded that the global behaviour of the water is similar as in the tests, but also that there are differences in the absolute load values. It should be noted that impact phenomena are sensitive to small

changes. In the model tests for instance a significant variation of impact loads was found even in regular waves, as can be seen in figure 18.
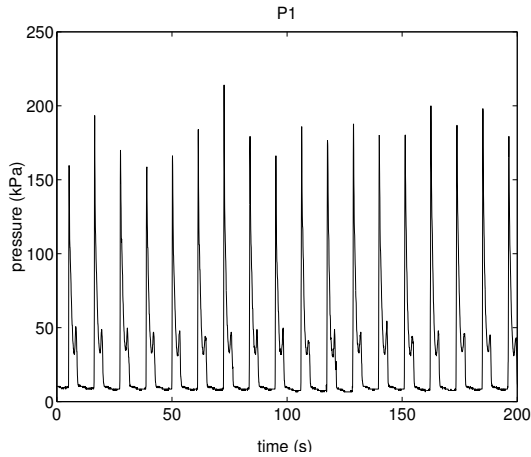

Figure 18: Sensitivity of the pressure in experiments

Looking at structure 1, at P1, the global shape of the pressure graphs correspond to each other, but in the maximum values of the pressure some differences occur. For P1, the maximum value in the simulation is 132 kPa, and for the tests, the mean value of the maxima, corresponding with a mean maximum height H3 of 4.93 m, is 167 kPa with a standard deviation of 13.1 kPa. The standard deviation is $\sigma = \sqrt{\frac{1}{N} \sum_{i=1}^{N} (p_i - \overline{p})}$, where N is the total number of measured maxima in the test and $\overline{p}$ is the mean value of the maxima. A difference of about 25 % in the maximum pressure is observed, but also the differences in the heights are about 25 %. At P2 almost nothing is observed in both simulation and test. P3 is left out in the figure, since the pressure was equal to the atmospheric value in both situations. A reason for the differences in the pressure may be the fact that the pressure in the simulation is determined in the cell centra and not exactly at the structure. Extrapolation of the pressure would be useful here, but since the solution near the structure is not very smooth, this is left out. It is also possible that the impact velocity is a bit different there, which may cause the difference in the pressure, since a small difference in the velocity means a squared difference in the pressure.

Looking at the total force in x-direction, the shape of the force graphs look similar, although the maximum force differs about 20-30 %.

To get an impression of the pressure distribution at the structure, in figure 19 the pressure distribution at the structure is plotted at times 2.5, 3, 3.5 and 4 seconds (the force peak is observed between 3 and 3.5 seconds). In figure 20 this pressure distribution is plotted as function of the height above deck for the situation at the centerline of the structure.
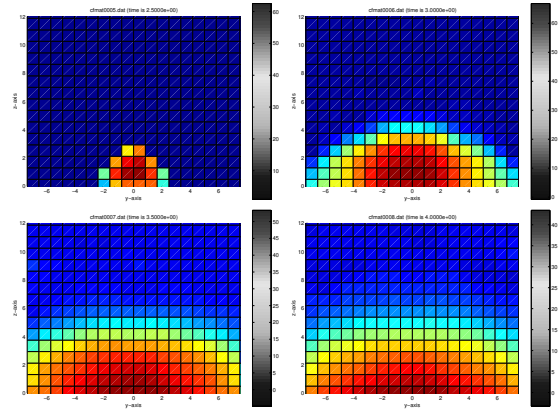

Figure 19: Pressure profile at structure at different moments in time
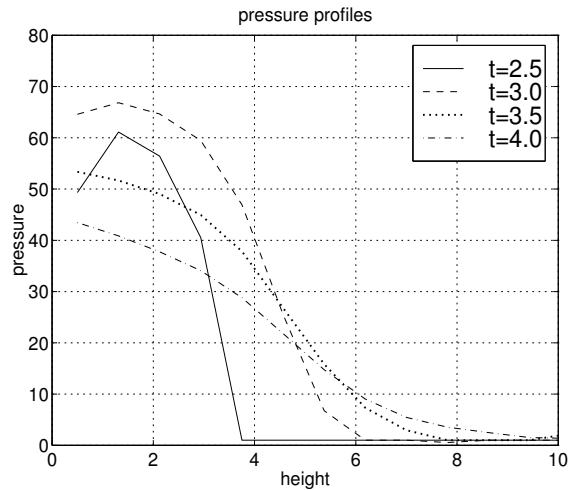

Figure 20: Pressure versus height at the centerline of the squared structure at different time steps

From this figure it becomes clear that initially the pressure is limited to the lower part of the structure (similar to the incoming waterheight). The pressure is high due to the fact that the momentum in the fluid is destroyed by the structure. In a later stage the pressure reaches also the higher positions at the structure, but the pressure is lower and only a result of the quasi-static water pressure due to the water in front of the structure.

For structures 2 and 3 the behaviour of the simulated pressure turned out to be very oscillatory, especially for the triangular structure. It is likely that these numerically observed pressure spikes should be attributed to numerical noise. However, to find out the nature of this noise, further investigation is required and compressible air flow has to be included in the model, see [8]. Also significant differences are visible in the level of the pressures, and the force turned out to be lower than the tests in structure 2 and 3. Some reasons for this may be:

- The initial conditions of the real situation, with the movement of the ship and the wate inflow, differ from the simulation.

- No pressure is defined in **B**-cells, which can cause some problems when using smooth geometries for the structures. In this case, for the computation of the force the pressure is taken from an **F**-cell close to this **B**-cell. This approach can cause a smaller force than desired on structures 2 and 3, since the pressure will increase when moving towards the structure. In the case of structure 1 this problem does not occur (see figure 21).
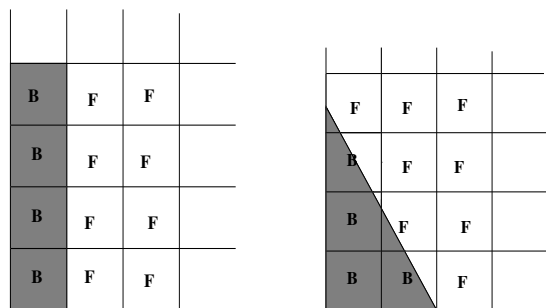

Figure 21: **F**-cells and **B**-cells near different structures

- The coarseness of the grid. One cell is about 1 x 1 x 1 meter, so for a pressure panel with a diameter of 2.7 meters, only two or three grid cells are contained in it.

These aspects are the subject of investigations at the moment.

CONCLUSIONS

In this research project the feasibility of numerically simulating green water loading by means of a Navier-Stokes model has been investigated. It was found that the global physical behaviour of the water on the deck is described quite well by the simulation. The high water 'tongue', as observed in the tests, is also visible in the simulation. Although differences appear between the tests and the simulations, the computed forces and pressures at the structures and at the deck are similar. The differences can partially be explained by numerical noise, on which some improvements will be made in the treatment of the **B**-cells in the future, and partially by physical differences. Referring to the purpose of this project, it can be concluded that further development of the simulation of green water is worth working on. Some aspects that will be investigated in the future are:

- Motion of the ship: A ship at sea is not fixed in space, but is moving in vertical and horizontal direction, this means that the geometry will be changing continuously.

- Creation of a wave field around the ship and realistic inflow (taking into account the effect of the bowflare). This will make the situation significantly more realistic.

References

1. Buchner, B., On the Impact of Green Water Loading on Ship and Offshore Unit Design, PRADS '95, September 1995. Seoul.

2. Buchner, B., A New Method for the Prediction of Non-Linear Relative Wave Motions, OMAE98, June 1998. Lisbon.

3. Buchner, B. and Cozijn, J. L., An investigation into the numerical simulation of green water, MARIN, February 1997.

4. Veldman, A. E. P., Numerieke Stromingsleer, March 1994. Lecture Notes.

5. Gerrits, J., "Three-dimensional liquid sloshing in complex geometries," Master's thesis, RUG, August 1996.

6. Botta, E. F. F. and Ellenbroek, M. H. M., "A modified sor method for the poisson equation in unsteady free-surface flow calculations," J. Comp. Phys. 60, 1985, pp. 119–134.

7. Loots, E., "Free surface flow in 3d complex geometries using enhanced boundary treatment," Master's thesis, RUG, June 1998.

8. Sabeur, Z. E., Cohen, J. E., Stephens, J. R. and Veldman, A. E. P., Investigation on Free Surface Flow Oscillatory Impact Pressures with the Volume of Fluid Method, In K.W. Morton and M.J. Baines, editors, *Numerical Methods for Fluid Dynamics*, volume VI. Oxford Science Publications, pp. 493-498.